Structural and Thermodynamic Analysis of a Conformationally Strained Circular Permutant of Barnase[†]

James S. Butler,[‡,§] Diana M. Mitrea,[§,||] Gregory Mitrousis,[§,||] Gino Cingolani,[||] and Stewart N. Loh*[,||]

Department of Biology, Massachusetts Institute of Technology, 77 Massachusetts Avenue, Cambridge, Massachusetts 02139, and Department of Biochemistry and Molecular Biology, State University of New York Upstate Medical University, 750 East Adams Street, Syracuse, New York 13210

Received January 9, 2009; Revised Manuscript Received March 2, 2009

ABSTRACT: Circular permutation of a protein covalently links its original termini and creates new ends at another location. To maintain the stability of the permuted structure, the termini are typically bridged by a peptide long enough to span the original distance between them. Here, we take the opposite approach and employ a very short linker to introduce conformational strain into a protein by forcing its termini together. We join the N- and C-termini of the small ribonuclease barnase (normally 27.2 Å distant) with a single Cys residue and introduce new termini at a surface loop, to create pBn. Compared to a similar variant permuted with an 18-residue linker, permutation with a single amino acid dramatically destabilizes barnase. Surprisingly, pBn is folded at 10 °C and possesses near wild-type ribonuclease activity. The 2.25 Å X-ray crystal structure of pBn reveals how the barnase fold is able to adapt to permutation, partially defuse conformational strain, and preserve enzymatic function. We demonstrate that strain in pBn can be relieved by cleaving the linker with a chemical reagent. Catalytic activity of both uncleaved (strained) pBn and cleaved (relaxed) pBn is proportional to their thermodynamic stabilities, i.e., the fraction of folded molecules. The stability and activity of cleaved pBn are dependent on protein concentration. At concentrations above ~2 μM, cleaving pBn is predicted to increase the fraction of folded molecules and thus enhance ribonuclease activity at 37 °C. This study suggests that introducing conformational strain by permutation, and releasing strain by cleavage, is a potential mechanism for engineering an artificial zymogen.

The ability to impose regulatory control on an enzyme in a reversible and well-defined manner is a primary goal of protein engineering studies. Enzymes require precise three-dimensional structure to be functional. Consequently, activity of an enzyme can in principle be modulated by disrupting its structure. Structural disruption can arise from small perturbations localized to the active site or from large-scale, global unfolding. In the cell, these changes can be effected by post-translational modification (e.g., phosphorylation), binding to ATP-dependent unfoldases, and proteolytic degradation (*1*−*3*). However, engineering proteins to respond to these cellular pathways remains a daunting task, and it is often desirable to retain the ability to exert control in the absence of these processes. Structural destabilization can be achieved in the laboratory by introducing point mutations which alter key catalytic residues or destabilize the enzyme. This approach, however, is generally not useful because the effects of mutation are permanent. Is there a means by which one can modulate protein structure such that function can be switched off and on?

Here, we explore the use of conformational strain as a potential mechanism for regulating enzyme function. The goal is to introduce strain into the native conformation, to distort the structure or destabilize it to the point of unfolding. Upon release of strain, the enzyme relaxes back to its native state and regains function.

We introduce conformational strain by circular permutation. Circular permutation covalently links the original termini of the protein and creates new ends at another location. This modification is shown schematically for a five-stranded β sheet in Figure 1A. The three-dimensional structure is typically preserved in all other aspects. Indeed, most previous studies attempt to preserve the stability and structure of the permuted protein. The new termini are placed in a solvent-exposed loop, and the original ends are bridged by a peptide long enough to span the distance observed in the wild-type (WT)[1] structure. These measures have produced stable and functional permutants of proteins such as GFP and related variants (*4, 5*), SH3 domains (*6*), PDZ domains (*7*), antibody light chain (*8*), and many others (e.g., refs *9*−*15*).

Here, we take the opposite approach and introduce strain by deliberately forcing the original termini together. This

[†] This work was supported by NIH Grant GM069755 to S.N.L.

* To whom correspondence should be addressed. E-mail: lohs@upstate.edu. Phone: (315) 464-8731. Fax: (315) 464-8750.

[‡] Massachusetts Institute of Technology.

[§] These authors contributed equally to this work.

[||] State University of New York Upstate Medical University.

[1] Abbreviations: Bn, barnase; CD, circular dichroism; F_{max}, wavelength of maximum fluorescence emission; NTCB, 2-nitro-5-thiocyanobenzoic acid; pBn, barnase circularly permuted with a Cys linker; pBn18, pBn with an 18-amino acid linker; pBnΔN$_2$, pBn with Ala1 and Gln2 deleted; pBnΔN$_3$, pBn with Ala1, Gln2, and Val3 deleted; SDS−PAGE, sodium dodecyl sulfate−polyacrylamide gel electrophoresis; WT, wild-type.

10.1021/bi900039e CCC: $40.75
Published on Web 03/04/2009

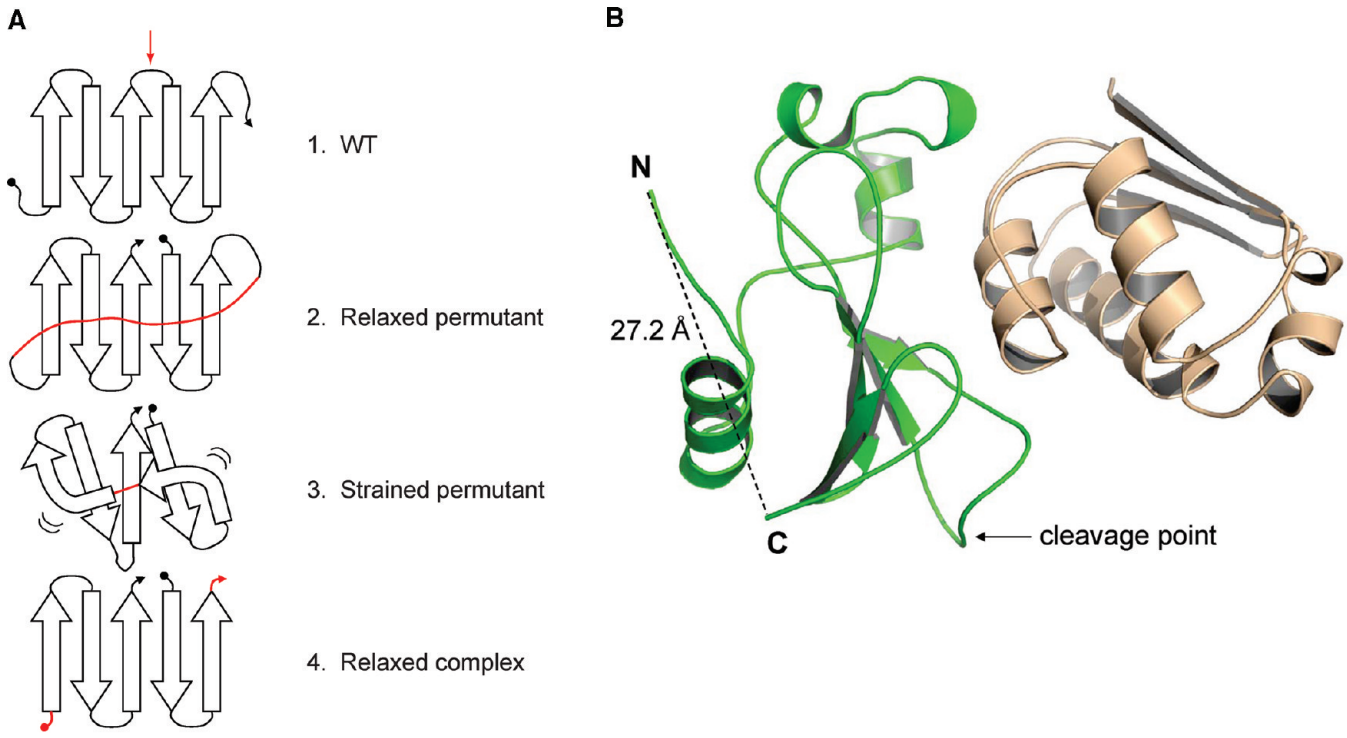

C

WT	AQVINTFDGVADYLQTYHKLPDNYITKSEAQALGWVASKGNLADVAPGKSIGGDIFSNREGKLPGKSGRTWREADINYTSGFRNSDRILYSSDWLIYKTTDHYQTFTKIR
BnΔN$_2$	--VINTFDGVADYLQTYHKLPDNYITKSEAQALGWVASKGNLADVAPGKSIGGDIFSNREGKLPGKSGRTWREADINYTSGFRNSDRILYSSDWLIYKTTDHYQTFTKIR
BnΔN$_3$	---INTFDGVADYLQTYHKLPDNYITKSEAQALGWVASKGNLADVAPGKSIGGDIFSNREGKLPGKSGRTWREADINYTSGFRNSDRILYSSDWLIYKTTDHYQTFTKIR
pBn	SGRTWREADINYTSGFRNSDRILYSSDWLIYKTTDHYQTFTKIRCAQVINTFDGVADYLQTYHKLPDNYITKSEAQALGWVASKGNLADVAPGKSIGGDIFSNREGKLPGK
pBnΔN$_2$	SGRTWREADINYTSGFRNSDRILYSSDWLIYKTTDHYQTFTKIRC--VINTFDGVADYLQTYHKLPDNYITKSEAQALGWVASKGNLADVAPGKSIGGDIFSNREGKLPGK
pBnΔN$_3$	SGRTWREADINYTSGFRNSDRILYSSDWLIYKTTDHYQTFTKIRC---INTFDGVADYLQTYHKLPDNYITKSEAQALGWVASKGNLADVAPGKSIGGDIFSNREGKLPGK
pBn18	SGRTWREADINYTSGFRNSDRILYSSDWLIYKTTDHYQTFTKIR*AQVINTFDGVADYLQTYHKLPDNYITKSEAQALGWVASKGNLADVAPGKSIGGDIFSNREGKLPGK
*	(GGS)$_5$GTM

FIGURE 1: Circular permutation-induced strain mechanism. (A) Effect of permuting a hypothetical five-stranded β sheet using progressively shorter linker peptides. N- and C-termini are designated by a circle and an arrow, respectively. The WT protein (structure 1) is permuted using a long peptide linker (red line). New termini are generated at the loop connecting strands 3 and 4 (red arrow). The resulting relaxed permutant (structure 2) is stable and active. A peptide linker shorter than the original N-terminal−C-terminal distance is employed in structure 3 to generate the strained permutant. Depending on the extent of strain, the protein may simply be destabilized, folded but distorted such that activity is diminished, or unfolded. Cleavage of the short linker relieves strain and allows the protein to refold as a complex (structure 4). (B) X-ray structure of WT Bn (green) complexed with the competitive inhibitor barstar (peach) (*44*). The locations of new termini introduced by permutation, and the $C_\alpha-C_\alpha$ distance between original termini, are indicated. (C) Amino acid sequences of Bn variants used in this study. Amino acids are numbered according to the WT sequence. Residues 1−66 are colored blue, residues 67−110 red, and linker residues boldface black.

mechanism is shown schematically in Figure 1A. If the WT protein (structure 1) is permuted with a long linker, the resulting permutant (structure 2) is relaxed, relatively stable, and functional. Permutation with a short connecting peptide introduces conformational strain (structure 3). The magnitude of strain is expected to depend on the distance discrepancy between the termini of the WT structure and the ends of the new surface loop in the permuted structure. If that disparity is small, then strain may destabilize the protein without appreciably perturbing its structure. A larger discrepancy may result in distortion of the active site structure such that activity is diminished or lost. In the extreme case, the new covalent linkage may compress the original termini to the point where it is no longer possible for the protein to remain folded. Cleaving the linker by chemical or enzymatic means is then envisioned to allow the original termini to relax to their preferred positions, permitting the protein to refold as a complex of two fragments (structure 4).

We test the permutation-strain mechanism using the bacterial ribonuclease barnase (Bn). Bn is a suitable target because it is small, stable, and known to unfold reversibly under a variety of conditions, including after it has been cleaved into two fragments (*16, 17*). In addition, its enzymatic activity is toxic to both prokaryotic and eukaryotic cells, a feature which makes it of potential therapeutic interest (*18, 19*). Using Bn as a model system, we ask two questions. Can permutation-induced strain significantly perturb protein structure? If so, can we reverse the perturbation such that enzyme function can be controlled?

To address those issues, it is necessary to understand how the native structure responds to permutation-induced strain. Are structural changes localized to the nascent loop and termini, or are they distributed throughout the protein? How much distortion can be tolerated without global unfolding? How robust is the native fold? We pursue these structural questions by X-ray crystallographic studies of a strained Bn permutant in complex with the natural inhibitor barstar.

EXPERIMENTAL PROCEDURES

Protein Expression and Purification. Bn variants were coexpressed with barstar in *Escherichia coli* BL21(DE3).

Following induction with IPTG at 20 °C, cells were harvested by centrifugation and lysed with a small amount of lysozyme. The soluble Bn−barstar complex was precipitated from the lysis supernatant by addition of 90% ammonium sulfate. The pellet was resuspended in 20 mM sodium acetate (pH 5.0) and 0.1 M NaCl, and the complex was purified on an Sephacryl S200 size-exclusion column (GE Healthcare) using the same buffer. The complex was then denatured in 9 M urea and 20 mM Tris (pH 7.5) and loaded onto a DE52 column. Bn present in the flow-through was judged to be >95% pure by SDS−PAGE. Barstar was retained on the column and discarded. Protein solutions were dialyzed extensively against double-distilled water (4 °C), lyophilized, and stored at −20 °C.

NTCB cleavage experiments were performed as described previously (*20*). Briefly, lyophilized protein was resuspended in 10 mM HCl (600−700 μM) and reduced with 40 mM tris(2-carboxyethyl)phosphine. The protein solution was then desalted into 10 mM HCl using a Sephadex G-25 column. Cyanylation was carried out by incubating the protein with a 25-fold excess of NTCB for 2 h at 37 °C in 85 mM Tris (pH 8.4) and 5.4 M GdnHCl. We performed cleavage by adjusting the pH to 10.0 with concentrated NH_4OH and incubating the sample for 20 h at 37 °C. The reaction was quenched by excess β-mercaptoethanol, and the solution was dialyzed extensively against ddH_2O. Fragments were purified using a C4 HPLC column (Hamilton) and a water/acetonitrile (0.1% trifluoroacetic acid) gradient.

Thermodynamic Measurements. Stock solutions were prepared daily by dissolving lyophilized proteins in 6 M urea (100−200 μM Bn) to break up any aggregates that may have formed during dialysis and freeze-drying. Working solutions for urea denaturation experiments were prepared by rapid dilution into ice-cold 20 mM sodium acetate (pH 5.0), 0.1 M NaCl, 2 mM β-mercaptoethanol, and the same buffer containing 6 M urea (final Bn concentration of 1 μM). Experimental samples were made by mixing these solutions using a Hamilton 500B diluter. Final urea concentrations were measured by the index of refraction (*21*). Samples were incubated for at least 3 h at 10 °C prior to fluorescence measurements. Fluorescence data were recorded at 10 °C using 280 nm excitation with excitation and emission band-pass values of 2 and 3 nm, respectively. Data were fit to the linear extrapolation equation using Kaleidagraph (version 3.6, Synergy software). Samples for thermal denaturation experiments were prepared as described above, except the protein concentration was increased to 2−3 μM for CD analysis. Data were normalized to fraction unfolded by manually fitting baselines to a linear equation and assuming a two-state unfolding reaction. Fragment binding was monitored by mixing the 1−66 and 67−110 peptides at a 1:1 ratio and fitting the F_{max} data to a 1:1 binding model using Origin 7 (www.originlab.com). The F_{max} value of the unfolded state was calculated by adding fluorescence spectra of the individual peptides which were recorded separately; this value was fixed in the curve fits. The F_{max} value of the native state was obtained from fitting the 10 °C data set in which the native baseline is well-established. F_{max} parameters were then constrained to those values for data sets in which the baselines were not fully resolved. Fluorescence and CD data were collected on Jobin-Yvon/SPEX Fluoromax-3 and Aviv model 202 instruments, respectively.

RNase Activity Assays. Torula yeast RNA hydrolysis assays were performed as described previously (*22*). Briefly, samples containing enzymes at the indicated concentrations were incubated at either 10 or 37 °C for 10 min. A 1:10 dilution of 20 mg/mL yeast RNA (Sigma) was added, and the reaction was allowed to progress at the indicated temperature. $HClO_4$ was added after a variable time to quench the reaction and precipitate undigested RNA. After centrifugation, the concentration of soluble RNA was measured by absorbance at 260 nm on a Varian Cary-1 spectrophotometer.

Crystallization and Structure Determination. The pBn−barstar complex was crystallized using the hanging drop vapor diffusion technique in the presence of 15−20% PEG 4000 and 100 mM NaCl (pH 7.5). Crystals of the pBn−barstar complex grew at 4 °C in clusters of thin plates, which were manually fragmented to generate individual small plates suitable for X-ray data collection. Several crystals were screened for diffraction at National Synchrotron Light Source (NSLS) beamline X6A as well as Cornell High Energy Synchrotron Source (CHESS) beamline A-1. The best diffraction data were collected at the CHESS A-1 station on a Quantum Q4 CCD detector. Diffraction data were reduced to intensities using the programs of the HKL2000 suites (*23*). Crystals belong to space group *P*1 with four pBn−barstar complexes in the asymmetric unit and diffracted X-rays to 2.15 Å resolution.

The structure was determined by the molecular replacement method using the WT Bn−barstar complex (Protein Data Bank entry 1BRS) as the search model. The search model, which represents only one-fourth of the triclinic cell, was searched in the asymmetric unit by computing cross-rotation and translation searches using the likelihood-based molecular replacement approach, as implemented in PHASER (*24*). Several searches were carried out using a minimum resolution of 15 Å and a maximum resolution ranging from 3.5 to 5.5 Å. Remarkably, all searches converged to one unique solution, with four pBn−barstar complexes in the asymmetric unit. The initial solution was refined in CNS (*25*) using rigid body refinement, simulated annealing, and grouped *B*-factor refinement to $R_{free} \sim 35\%$ (calculated using 5% of the observed reflections). The four pBn molecules in the asymmetric unit were rebuilt in $2F_o - F_c$ and $F_o - F_c$ electron density difference maps using the program Coot (*26*). The four pBn−barstar complexes in the asymmetric unit are designated 1, 2, 3, and 4. The engineered loop region is clearly visible in complex 1 and was modeled only in that structure. Several rounds of positional refinement in Refmac5, alternated with manual rebuilding, lowered R_{free} to 28%. After the majority of the protein model had been built, solvent was modeled in Coot by adding 372 water molecules to well-defined circular peaks of density, visible in $F_o - F_c$ electron density difference maps contoured to 2.5σ.

To analyze the flexibility of the pBn−barstar model, translation/libration/screw motion determination (TLSMD) analysis of the isotropically refined model was carried out using the TLS server (http://skuld.bmsc.washington.edu/~tlsmd/). This analysis partitioned the crystallographic pBn−barstar model into multiple segments, which were modeled as rigid bodies undergoing TLS vibrational motion (*27, 28*). A maximum of seven TLS groups calculated by the TLSMD server were used to further refine the structure

in Refmac5 using the TLS+ restrained refinement mode. This procedure lowered the final R_{work} and R_{free} of the crystallographic model to 20.5 and 25.0%, respectively, using all reflections between 30 and 2.25 Å resolution. The average *B*-factor for the four pBn−barstar models is 36−38 Å^2, which is close to the value of ~37 Å^2 extrapolated from the Wilson plot. A check of stereochemistry by PROCHECK (*29*) revealed that 87.1 and 12.6% of the model residues fall in allowed and generously allowed regions of the Ramachandran plot, respectively. Only 0.1% of the model residues (residue 47) is in disallowed regions. All structural figures were made using Pymol (*30*). Coordinates for the pBn−barstar model were deposited in the Protein Data Bank as entry 3DA7.

RESULTS

Nomenclature and Design of Permutants. We permuted Bn between Lys66 and Ser67, which lie at the tip of a large solvent-exposed loop (Figure 1B). This site was chosen because the 1−68 and 69−110 fragments refold to form the most stable complex among several pairs tested (*16*). The $C_\alpha-C_\alpha$ distance between the first (Ala1) and last (Arg110) amino acids is 27.2 Å. At least nine amino acids in a typical random coil conformation would be required to span that distance. In this study, we bridge the termini with a single amino acid (Cys) to facilitate cleavage by 2-nitro-5-thiocyanobenzoic acid (NTCB). To remain consistent with existing literature, amino acids in Bn permutants are numbered according to the WT sequence. For example, all permutants begin with Ser67 and end with Lys66. The bridging amino acid is designated Cys0. Permutants are designated by the prefix "p".

Four permutants were constructed (Figure 1C). pBn simply links Ala1 and Arg110 with Cys0. We then deleted Ala1 and Gln2 and Ala1, Gln2, and Val3 in an effort to further increase conformational strain. These variants are designated pBnΔN$_2$ and pBnΔN$_3$, respectively. Ala1 and Gln2 are disordered in the X-ray crystal structure of free Bn (*31*), which suggests that their deletion may have little effect on the stability of Bn or that of the cleaved complex. In contrast, these residues may play a larger role in the stability of pBn, if they act as a flexible extension to relieve strain between the original termini. To represent permuted Bn in its unstrained state, we joined Ala1 and Arg110 with the 18-amino acid linker (GGS)$_5$GTM to generate pBn18. Although the 27.2 Å N-to-C gap can in principle be bridged by approximately nine residues, that distance is measured in a straight line and does not take into account the need for the linker to curve around the outer surface of the protein. We doubled the theoretical number of amino acids to ensure that the control permutant is fully relaxed. If the nascent loop is too long, then the protein will be destabilized by loop closure entropy loss (*32, 33*). We reasoned that 18 amino acids is an appropriate balance between strain relief and entropic destabilization.

One concern when introducing conformational strain is that the molecule will relieve strain by undergoing a three-dimensional domain swap to generate dimers or higher-order oligomers (*34*−*36*). As part of the purification protocol, the samples are loaded onto a size exclusion column. pBn variants elute at approximately the same position as WT Bn (not shown). In addition, we do not observe evidence of domain swapping in the X-ray structure of pBn. These findings indicate that pBn variants are monomeric in solution.

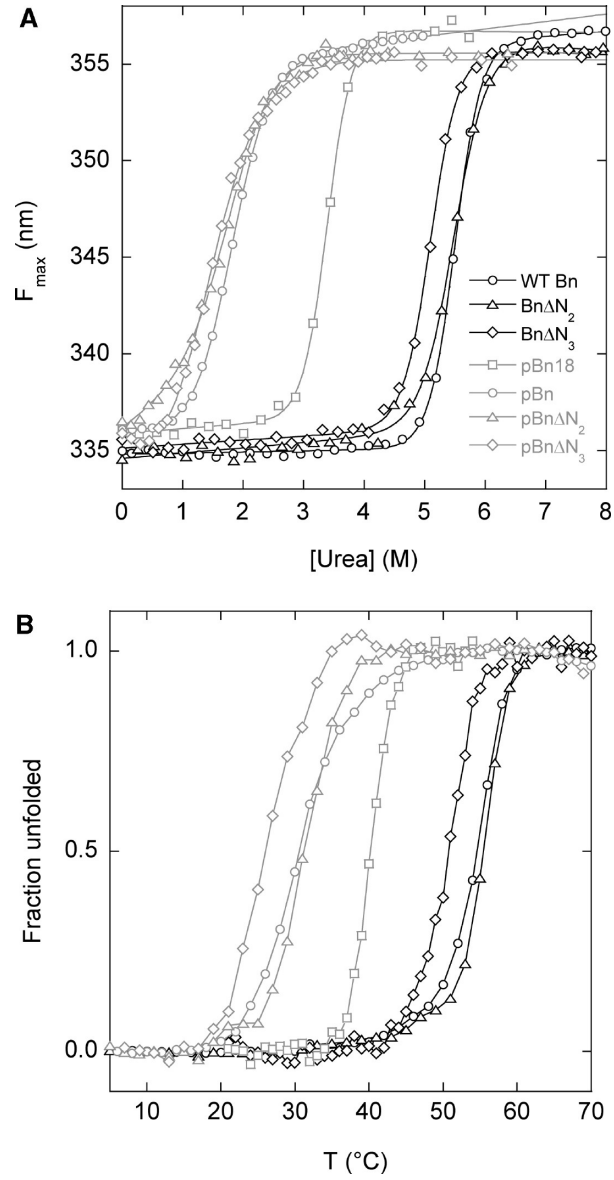

FIGURE 2: Thermodynamic stability of Bn variants. (A) Urea-induced denaturation curves monitored by Trp fluorescence at 10 °C. Lines are best fits of the data to the two-state linear extrapolation equation. (B) Thermal denaturation curves monitored by CD ellipticity at 230 nm. Symbols are the same as in panel A. Data are normalized assuming two-state unfolding. Lines are meant to guide the eye only.

Effect of Permutation on Stability. We first determined the stabilities of nonpermuted Bn variants. Figure 2A shows urea-induced equilibrium unfolding curves monitored by the wavelength of maximum fluorescence (F_{max}) of the three Trp residues (Trp35, Trp71, and Trp94). The native and unfolded forms of Bn exhibit characteristic F_{max} values of 335 and 355 nm, respectively (*37*). All unfolding transitions are reversible and are fit adequately by the two-state linear extrapolation equation $\Delta G = \Delta G^{H_2O} - m[\text{urea}]$, where ΔG^{H_2O} is the free energy change between native and unfolded states in the absence of denaturant and m is proportional to the change in the accessible surface area between states (*38*). Thermodynamic parameters are listed in Table 1. As expected, deleting Ala1 and Gln2 has a minimal effect on

Table 1: Thermodynamic Parameters and Catalytic Rates for Bn Variants

	ΔG^{H_2O} (kcal/mol)[a]	m (kcal mol^{-1} M^{-1})[a]	C_m (M)	T_m (°C)	k_{cat}, 10 °C[b] [M nucleotide (M enzyme)$^{-1}$ s^{-1}]	k_{cat}, 37 °C[b] [M nucleotide (M enzyme)$^{-1}$ s^{-1}]
WT Bn	14.0 ± 0.4	2.5 ± 0.1	5.5	54.9	6.6 ± 0.2	22 ± 0.6
BnΔN$_2$	11.2 ± 0.2	2.0 ± 0.1	5.5	55.7	4.6 ± 0.3	11 ± 0.7
BnΔN$_3$	12.8 ± 0.3	2.5 ± 0.1	5.1	53.3	3.9 ± 0.2	17 ± 0.8
pBn18	10.2 ± 0.8	3.0 ± 0.2	3.1	40.2	3.3 ± 0.4	20 ± 0.9
pBn	3.0 ± 0.1	1.5 ± 0.05	2.0	30.2[d]	3.3 ± 0.3	2.2 ± 0.1
pBnΔN$_2$	2.2 ± 0.1	1.3 ± 0.05	1.7	31.9[d]	1.4 ± 0.2	1.2 ± 0.07
pBnΔN$_3$	2.2 ± 0.3	1.5 ± 0.1	1.4	26.2[d]	1.4 ± 0.1	0.77 ± 0.02
1−66/67−110	NM[c]	NM[c]	NM[c]	35.6[e]	2.9 ± 0.1	1.4 ± 0.04
3−66/67−110	NM[c]	NM[c]	NM[c]	NM[c]	2.2 ± 0.1	NM[c]
4−66/67−110	NM[c]	NM[c]	NM[c]	NM[c]	1.4 ± 0.1	NM[c]

[a] The error is the standard deviation of three measurements. [b] Error reported from curve fitting results. [c] Not measured. [d] Thermal unfolding is irreversible. [e] Peptide concentration of 3 μM.

Bn. BnΔN$_2$ (ΔG^{H_2O} = 11.2 kcal/mol, and C_m = 5.5 M) is only slightly less stable that WT Bn (ΔG^{H_2O} = 14.0 kcal/mol, and C_m = 5.5 M), where C_m is the midpoint of the transition. Truncating Val3 does not result in additional destabilization. BnΔN$_3$ exhibits ΔG^{H_2O} and C_m values of 12.8 kcal/mol and 5.1 M, respectively.

We next asked if permuting Bn can introduce conformational strain and whether destabilization can be intensified by truncating amino acids from the original N-terminus. pBn18, which represents the relaxed state, is moderately destabilized (ΔG^{H_2O} = 10.2 kcal/mol, and C_m = 3.1 M) compared to WT Bn (Figure 2A). Reducing the linker to a single amino acid produces two effects. First, the stability drops substantially (ΔG^{H_2O} = 3.0 kcal/mol, and C_m = 2.0 M for pBn). Second, the unfolding transition becomes less cooperative. The m value of pBn is 1.5 kcal mol^{-1} M^{-1}, compared to 2.5−3.0 kcal mol^{-1} M^{-1} for pBn18 and the nonpermuted Bn variants. This decrease can be caused by a reduction in the accessible surface area of the native state, an increase in the surface area of the denatured state, or both. Alternately, it may result from partially folded forms being populated in the unfolding transition. In either case, it appears that shortening the linker to a single residue imparts considerable strain into the permuted form. Surprisingly, truncating Ala1−Val3 does not dramatically intensify strain. pBnΔN$_2$ and pBnΔN$_3$ are only slightly less stable than pBn, and all of these variants exhibit native F_{max} values similar to that of WT Bn.

We further characterized stability changes by thermal denaturation experiments monitored by circular dichroism (CD). WT Bn, BnΔN$_2$, BnΔN$_3$, and pBn18 all denature reversibly (Figure 2B). Melting temperatures (T_m) of BnΔN$_2$ (55.7 °C) and of BnΔN$_3$ (53.3 °C) are similar to that of WT (54.9 °C), whereas the T_m of pBn18 is reduced (40.2 °C). This result confirms that truncating the first three N-terminal residues has little effect on stability, and that permutation with a long linker is moderately destabilizing. The short linker permutants again exhibit distinctly different behavior. Thermal unfolding is irreversible for pBn, pBnΔN$_2$, and pBnΔN$_3$, and apparent T_m values (26.2−31.9 °C) are markedly lower than those of their nonpermuted counterparts.

Stability of Cleaved pBn. Cleavage of the Cys linker is expected to relieve strain and allow the protein to relax to its preferred conformation (Figure 1A, structure 4). Because folding of the fragments is coupled to their binding, the stability of the complex increases with peptide concentration. Whether the fraction of folded enzyme increases or decreases upon cleavage consequently depends on protein concentration. For example, the ΔG^{H_2O} of the complex formed by the 1−68 and 69−110 fragments was determined to be 6.3 kcal/mol at a peptide concentration of 15 μM and 25 °C (*16*). This value is considerably higher than the ΔG^{H_2O} value for uncleaved pBn measured at 10 °C [3.0 kcal/mol (Table 1)]. Thus, cleaving pBn will theoretically increase the amount of folded enzyme at a protein concentration of 15 μM. However, the difference is not significant, since >99% of pBn molecules are already folded in the absence of cleavage. The increase in stability upon cleavage is anticipated to be greater at higher temperatures where pBn is unstable.

To determine the stability of cleaved pBn, we processed pBn with NTCB, purified the 1−66 and 67−110 fragments using reverse-phase HPLC, and measured the apparent K_d for binding and/or folding using Trp fluorescence. The fragments bind with a K_d of 30 nM at 10 °C and yield a complex with an F_{max} value (336 nm) similar to that of WT (Figure 3A). Binding affinity decreases with an increase in temperature; K_d increases to 0.13, 1.9, and 60 μM at 20, 30, and 37 °C, respectively. These findings are consistent with the high stability of the 1−68/69−110 complex at 25 °C reported by Neira et al. (*16*). To illustrate how pBn stability is predicted to increase upon cleavage, Figure 3B plots the binding isotherm for the 1−66 and 67−110 peptides at 37 °C. Approximately 10% of pBn molecules are folded at this temperature (Figure 2B). Figure 3B shows that cleaving pBn will increase or decrease the fraction of folded protein depending on the protein concentration. The crossover point is ∼2 μM protein. Above this concentration, cleavage of pBn will produce a net increase in the number of folded molecules and a concomitant enhancement of activity.

Ribonuclease Activity Assays. To test the predictions described above, we characterized the functional status of Bn variants by monitoring hydrolysis of genomic RNA from Torula yeast (*22*). All variants, both nonpermuted and permuted, are folded at 10 °C (Figure 2A). Any changes in activity at this temperature must therefore be caused by structural perturbations and not by unfolding. Apparent k_{cat} values are calculated from the slopes of the linear fits of the data in Figure 4, which were acquired at a saturating substrate concentration (2 mg/mL). Since the RNA substrate is heterogeneous, k_{cat} is expressed as molar nucleotide per molar enzyme per minute, using an average extinction coefficient of OD_{260} = 0.11 mM nucleotide cm^{-1}. k_{cat}values of all nonpermuted proteins and pBn18 are within 60% of the WT figure (Figure 4 and Table 1). Deleting Ala1−Val3, as well

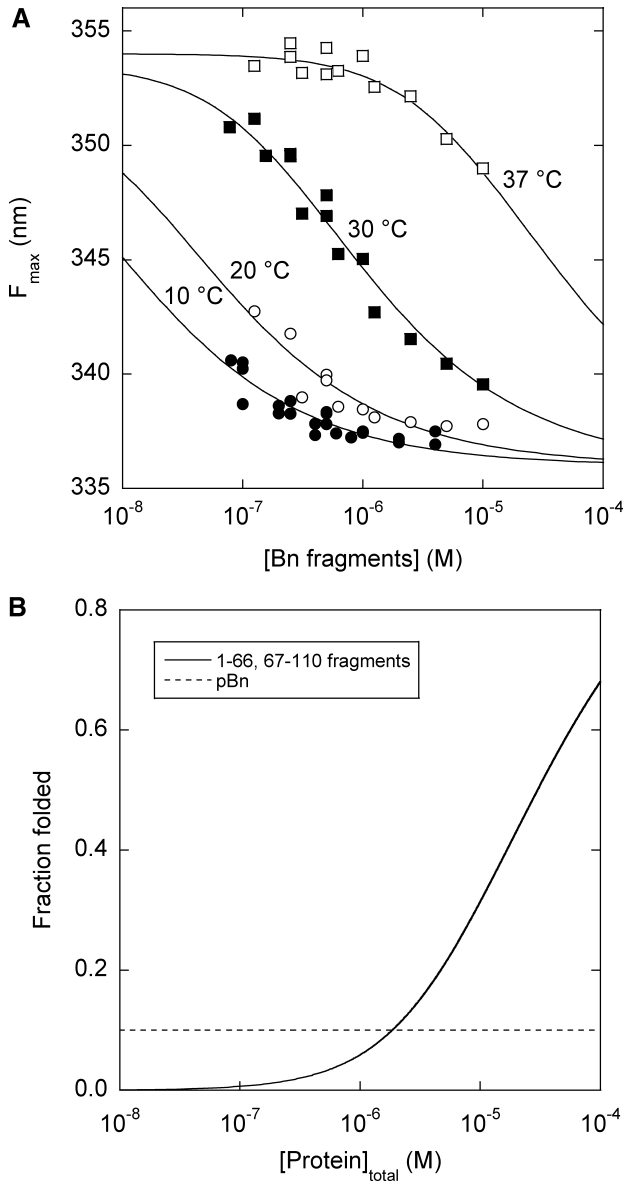

FIGURE 3: Binding and refolding of the 1−66 and 67−110 fragments of Bn. (A) Temperature dependence of binding, monitored by Trp fluorescence. Fragments were mixed in a 1:1 ratio at the concentrations indicated. Lines are best fits of the data to the 1:1 binding equation. Fitted K_d values are 30 nM (10 °C), 0.13 μM (20 °C), 1.9 μM (30 °C), and 60 μM (37 °C). (B) Binding isotherm of Bn fragments at 37 °C, calculated using a K_d of 60 μM. The dashed line depicts the values for uncleaved pBn.

as permuting with a long linker, does not compromise the integrity of the active site.

pBn, pBnΔN$_2$, and pBnΔN$_3$ are only slightly less active then their nonpermuted counterparts (by factors of 2.0, 3.4, and 2.7, respectively). The short linker permutants thus appear to be strained but still functional; there is no major distortion of the active site. We cleaved pBn, pBnΔN$_2$, and pBnΔN$_3$ with NTCB to generate the 1−66/67−110, 3−66/67−110, and 4−66/67−110 complexes, respectively. All three peptide pairs bind and refold to yield functional complexes (Table 1). The activity of each complex is comparable to that of the uncleaved parent permutant, signifying that cleaving the surface loop around Lys66 and Ser67 has little effect on catalysis.

As expected from the melting curves of Figure 2B, WT Bn, BnΔN$_2$, BnΔN$_3$, and pBn18 hydrolyze RNA with

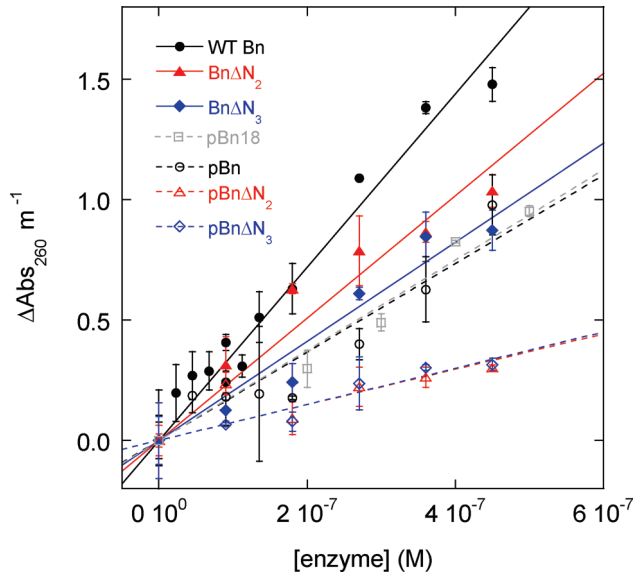

FIGURE 4: RNase activity assays of Bn variants at 10 °C. Hydrolysis of Torula yeast genomic RNA is monitored by the change in absorbance at 260 nm. Error bars are standard deviations of three measurements.

Table 2: X-ray Data Collection and Refinement Statistics

data set name	pBn−barstar
beamline	CHESS-A1
space group	*P*1
resolution (Å)	30−2.15
no. of reflections (total/unique)	719659/50783
unit cell (Å)	a = 38.88
	b = 80.24
	c = 81.92
angle (deg)	α = 88.10
	β = 76.98
	γ = 79.47
completeness[a] (%)	96.0 (95.2)
R_{sym}[b] (%)	10.9 (39.2)
$\langle I\rangle/\langle\sigma(I)\rangle$	29.9 (5.8)
Refinement Statistics	
resolution reflection used (Å)	30−2.25
no. of protein residues in the model	774
no. of water molecules	372
R-factor/R_{free}[c] (%)	20.5/25.0
rmsd for bond lengths (Å)	0.010
rmsd for bond angles (deg)	1.06
ϕ, ψ most favored (%)	87.1
ϕ, ψ additionally favored (%)	12.6
ϕ, ψ generously favored (%)	0.1
ϕ, ψ disallowed (%)	0.1
average B-factor (Å^2)	
Wilson B-factor	37.8
pBn−barstar complex 1	38.2
pBn−barstar complex 2	38.1
pBn−barstar complex 3	38.1
pBn−barstar complex 4	38.2
water	38.0

[a] Numbers in parentheses refer to the statistics for the outer resolution shell (2.23−2.15 Å). [b] $R_{sym} = \sum_{i,h}|I(i,h) - \langle I(h)\rangle|/\sum_{i,h}|I(i,h)|$, where $I(i,h)$ and $\langle I(h)\rangle$ are the ith and mean measurements of the intensity of reflection h, respectively. [c] R_{free} value calculated using 5% of the data.

comparable rates at 37 °C (Table 1). By contrast, increasing the temperature to 37 °C reduces the activity of the short linker permutants by 10-fold (pBn and pBnΔN$_2$) and 23-fold (pBnΔN$_3$), compared to the activities of their nonpermuted counterparts. This decrease appears to follow the trend in T_m values observed in Figure 2B. It thus likely reflects

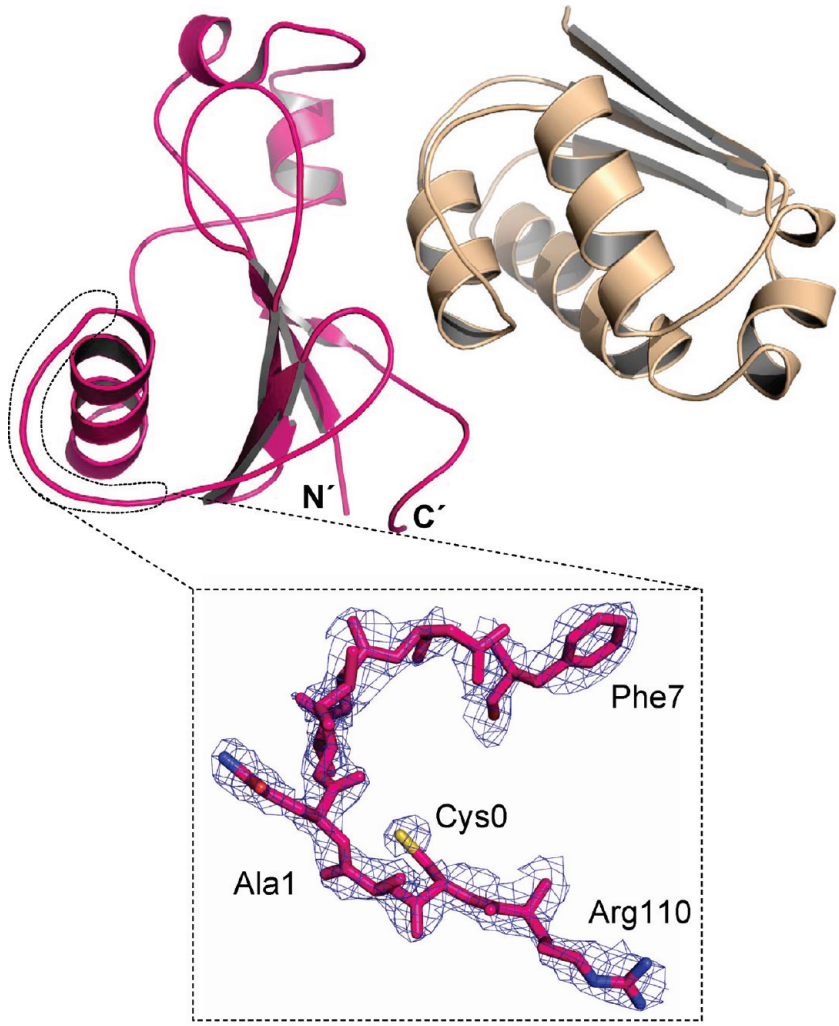

FIGURE 5: Crystal structure of pBn (magenta) bound to barstar (peach). The perspective is the same as in Figure 1B. The inset shows the $2F_o - F_c$ composite omit map of the linker loop, contoured at 1.5σ. Nascent termini introduced by permutation are designated N′ and C′.

the instability of the short linker permutants at elevated temperatures. Cleaving pBn results in an ~50% loss of activity at the enzyme concentrations employed in the assay (0.1−2.0 μM). This figure is in reasonable agreement with Figure 3B, which predicts that approximately 10% of pBn and 5% of the 1−66/67−110 complex are folded at 1 μM and 37 °C.

Crystallographic Analysis of pBn Bound to Barstar. To understand how Bn responds to permutation-induced conformational strain, we crystallized pBn complexed with its natural inhibitor barstar. A complete data set to 2.15 Å resolution was collected from a single small plate crystal cryo-protected in 30% glycerol. Diffraction analysis confirmed that pBn−barstar crystals belong to space group *P*1, with four pBn−barstar complexes in the asymmetric unit. The four complexes pack in the unit cell as two nonequivalent biheterodimers. Each of the two pBn−barstar heterodimers is generated by a local 2-fold noncrystallographic symmetry axis running between two barstar protomers, which pack their C-termini against each other by forming an inverted β-sheet between residues 85 and 90. However, no domain swap is observed between complexes in the asymmetric unit.

The structure was determined by the molecular replacement method using the structure of the wild-type Bn−barstar complex (PDB entry 1BRS) as the search model. The final model was refined to R_{work} and R_{free} values of 20.5 and 25.0%, respectively, using all reflections between 30 and 2.25 Å (Table 2). The final model average *B*-factor is ~37 Å^2, which is close to the *B*-factor of the X-ray data extrapolated from the Wilson plot. One of the four complexes (complex 1 in Table 2) in the triclinic unit cell shows clear density for the engineered permutation loop. This is likely due to slightly different packing environments in the crystal lattice. The four Bn molecules in the asymmetric unit are in similar but not identical conformations. Average C_α root-mean-square deviations (rmsds) of Bn in complex 1 compared to Bn in the other three complexes are 0.35, 0.84, and 0.43 Å. Barstar molecules superimpose more closely, with analogous rmsds of 0.15, 0.24, and 0.26 Å, respectively. Thus, the combination of different packing environments and the high plasticity of pBn (compared to barstar) is likely responsible for the unusual arrangement of the four pBn−barstar heterodimers in the triclinic unit cell.

The structure of pBn−barstar complex 1 is shown in Figure 5, in the same orientation depicted in Figure 1B for the WT Bn−barstar complex. The engineered loop spans 27.2 Å to bridge the original N- and C-termini of Bn. This loop exhibits clear density and, as conceived in the initial design, is fully exposed to solvent.

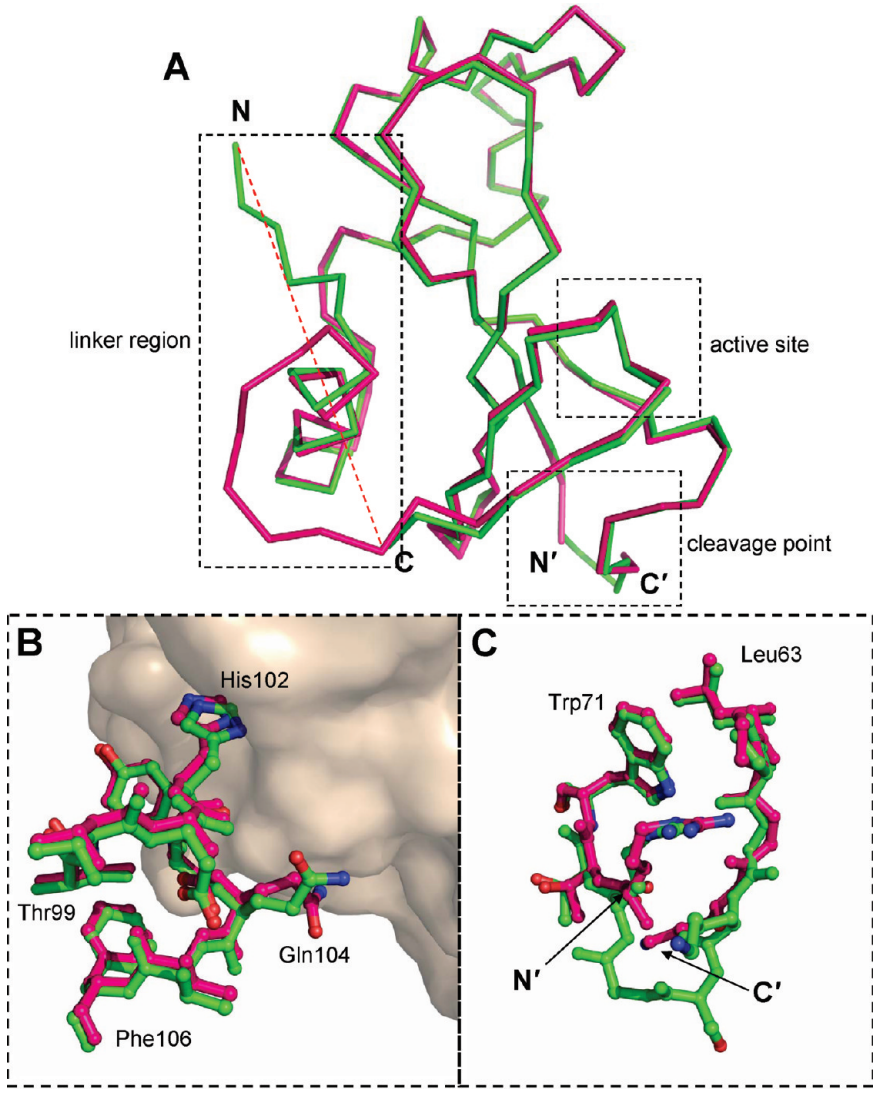

FIGURE 6: Superposition of pBn (magenta) and WT Bn (green) crystal structures. (A) Main chain atoms are shown in the same perspective as in Figure 1B. Boxes indicate regions of interest discussed in the text. (B) Close-up of the catalytic site, including the general acid His102. (C) Close-up of the surface loop that contains the nascent N′- and C′-termini (Ser67 and Lys66, respectively).

The structures of pBn (magenta) and WT Bn (green) are superimposed in Figure 6. A combination of dramatic and subtle structural rearrangements occurs as a result of permutation. Ala1−Thr6 at the N-terminus and Arg110 at the C-terminus join with Cys0 to form a linker connecting the N-terminal α-helix (residues 7−18) to the C-terminal β-strand (residues 105−108). Those two secondary structure elements display small main chain shifts relative to WT Bn, suggesting that they are indeed under stress. The boxed regions of Figure 6A highlight three locations of interest. Examination of the active site, a portion of which is shown in Figure 6B, reveals that the positions of the general acid (His102) and general base (Glu73, not shown) are unperturbed, as are most other residues in the active site. One exception is the side chain of Gln104, which is oriented differently in the two structures. This finding is consistent with kinetic measurements which find little difference in the rates of RNA hydrolysis between WT Bn and pBn (Figure 4).

Figure 6C expands the region containing the nascent termini. Because the surface loop is long, is flexible, and can accommodate insertion of several proteins (*34, 37, 39*), we surmised that nicking the loop between Lys66 and Ser67 would have little impact on structure. Not unexpectedly, the nascent N-terminal residues Ser67 and Gly68 are flexible and no electron density is observed. Trp71 and Leu63 immediately upstream and downstream of the nick site, respectively, superimpose well with the WT Bn structure.

Structural Basis for pBn Reorganization. How does Bn cope with permutation to minimize changes to its overall structural topology and maintain function? To address that question, we now focus on the most important region, the engineered permutation loop itself (Figure 7). The structure reveals that a dramatic structural rearrangement takes place to accommodate the new connection. Residues 1−6 unwind from the N-terminus and rotate to link to the C-terminus. Notably, at Thr6, the main chain pivots ~180° with respect to WT Bn. Despite the spatial reorganization of the first six residues as a result of the permutation, Phe7 adopts a similar conformation in pBn and WT Bn. The Phe7 side chain is buried deeply in a hydrophobic pocket. In that respect, Phe7 may act as a molecular hook to prevent the distortion exhibited by residues 1−6 from propagating into the N-terminal α-helix. On the other side of the permutation loop, the C-terminal β-strand is also slightly perturbed. Residues 102−109 experience small but significant shifts compared to WT Bn. The largest difference is seen for Arg110, which

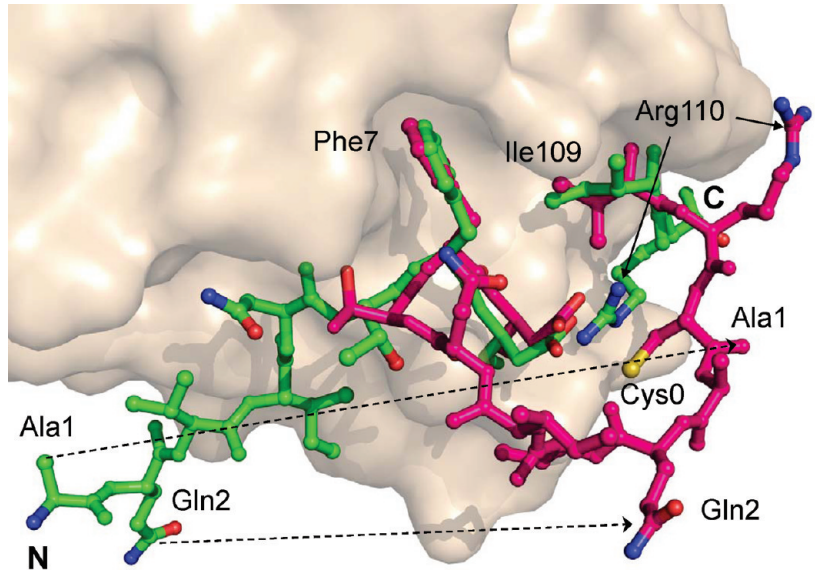

FIGURE 7: Structure of the linker region, showing the distribution of strain. Ala1, Gln2, and Arg110 are highlighted to illustrate the large shift in the positions of linker residues (Arg110-Cys0-Ala1-Gln2-Val3-Ile4-Asn5-Thr6) upon permutation. By contrast, side chains of residues Phe7 and Leu109 remain anchored in hydrophobic pockets.

engages in a bidentate salt bridge with Asp8 and Asp12 in the WT structure but loses these interactions in pBn, as it is forced to swing out and change direction to connect with the N-terminus.

The pBn structure thus suggests that Phe7 and Ile109 may be "anchor" residues. The side chains of Phe7 and Ile109 remain buried in hydrophobic pockets in the structures of pBn and WT Bn, whereas the intervening amino acids (Arg110-Cys0-Ala1-Gln2-Val3-Ile4-Asn5-Thr6) take up dramatically different positions. These eight amino acids effectively act as an extended linker to join the original termini. The positions of the anchor residues are envisioned to be critical for maintaining the structure and stability of Bn upon permutation. The $C_\alpha-C_\alpha$ distance between Phe7 and Ile109 is 8.8 Å in WT Bn and is reduced to 7.7 Å in pBn. This finding may explain why even the truncated permutants remain folded at 10 °C. That distance can be spanned by two or three amino acids. pBnΔN_2 and pBnΔN_3 contain six and five amino acids, respectively, between the anchor residues.

DISCUSSION

A general mechanism for regulating enzyme activity and protein function is modulation of its stability. The novelty of our approach is that instability is introduced by conformational strain, and that strain can be reversed in trans upon cleavage. A free energy diagram depicting this process for Bn (37 °C) is shown in Figure 8. The relaxed permutant pBn18 is somewhat less stable than WT Bn. Permutation with a short linker introduces strain sufficient to lower stability below the threshold level [$\Delta G^{H_2O} = 0$ (dashed line)], thereby attenuating catalytic activity. If one wishes to eliminate 99% of activity, then the permutant must possess a ΔG^{H_2O} value of −2.8 kcal/mol. The strain energy required to meet this condition is quite large in the case of WT Bn (16.8 kcal/mol at 10 °C). To reduce this energetic demand, it may be useful to introduce a destabilizing mutation into the core of the protein, which is expected to destabilize nonpermuted and permuted forms to comparable extents.

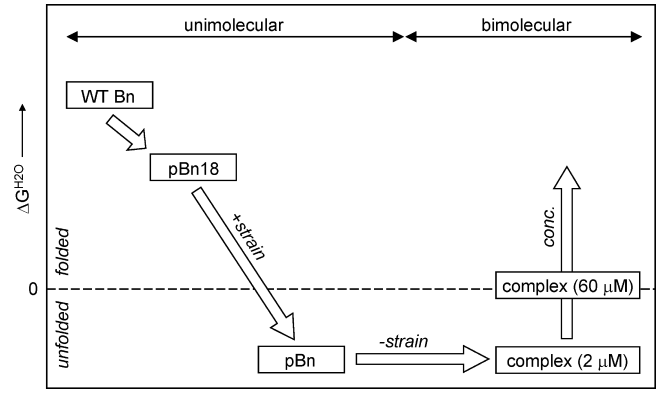

FIGURE 8: Free energy diagram of the permutation strain mechanism for Bn at 37 °C. Arrows are not drawn to scale.

After cleavage, the vertical position that the complex attains on the free energy diagram depends on protein concentration. The position of the 1−66/67−110 complex rises above that of uncleaved pBn at a peptide concentration of ∼2 μM (37 °C) and crosses the threshold line at ∼60 μM (Figure 3B). One way to stabilize the complex and remove the dependence on protein concentration is to reduce folding from a bimolecular process to a unimolecular one. This can in principle be achieved by introducing a disulfide bridge to cross-link the fragments. In our design, the most straightforward placement of Cys residues is at the nascent termini (Ser67 and Lys66), as these residues are naturally close in the native structure. Using this strategy, we can hope that the stability of the cleaved complex will be similar to that of the WT enzyme and independent of protein concentration.

The extent of permutation-induced strain is expected to depend primarily on the distance between N- and C-termini in the WT structure. However, our data indicate that it also depends on the rigidity/flexibility of the structure around the termini, and the extent to which N- and C-terminal amino acids are involved in stabilizing interactions. The first six amino acids of Bn as well as the last are able to detach from their positions in the WT structure, loop back, and form a

flexible tether to join the termini in the permutant. The anchor points appear to be the side chains of Phe7 and Ile109. There are two likely explanations for how the permutants are able to remain folded. First, the relevant N-to-C distance is not the 27.2 Å gap between Ala1 and Arg110, but rather the much shorter distance of 8.8 Å between anchor residues. Second, some of the terminal amino acids are able to change their conformation in the permutant, extend the single-Cys linker, and relieve strain.

Our strategy of regulating RNase activity by permutation and cleavage resembles that taken in several earlier studies by Raines and co-workers (*40*−*42*). They permuted bovine RNase A using 14- and 15-residue linkers containing cleavage sequences recognized by NS3 protease and HIV-1 protease, respectively. k_{cat}/K_M increased 50−100-fold after proteolytic cleavage. However, their mechanism for suppressing activity in the uncleaved state is distinct from ours. The RNase A permutant exhibited high conformational stability in both cleaved and uncleaved forms. The 14- and 15-residue linkers inhibited substrate binding by partially occluding the active site. Thus, their approach relies on steric blockage while ours depends on conformational strain. Each has its own advantages. The former allows one to permute with a long linker, which permits choice of cleavage sequences and facilitates access by the protease. The drawback is that active site occlusion cannot be assured as a general outcome. The conformational strain mechanism is applicable to all proteins, but its success depends on N-to-C length (as well as the structural factors discussed above). These considerations limit the length of the linker peptide used to permute the protein.

To what extent can the strain mechanism be applied to other enzymes? Our results suggest that many proteins may be amenable to this approach. Permutation with long linkers is generally well-tolerated, and we have demonstrated that the use of short linkers dramatically destabilizes the permuted form. Destabilization is expected to be particularly effective if the terminal residues are involved in extensive secondary or tertiary interactions. We note that anchor residues Trp7 and Ile109 correspond to the start of the N-terminal α-helix and the end of the C-terminal β-strand, respectively. The cooperative nature of protein structure suggests that if any individual element of secondary structure is disrupted, then a protein is likely to unfold or become severely destabilized. For pBn, pBnΔN_2, and pBnΔN_3, the five to eight amino acids between Ile109 and Trp7 absorb the permutation-induced distortion and prevent it from propagating to the N-terminal α-helix and the C-terminal β-sheet. Proteins whose secondary structures extend all the way to their ends may lack this compensatory capability.

To be activated upon cleavage, the nicked protein must be slow to dissociate into fragments, or the fragments must be able to bind and refold (or both). Numerous proteins possess these characteristics. The latter property forms the basis of the protein fragment complementation assay (PCA) used to probe protein−protein interactions in vivo. Proteins which have been successfully used for PCA include dihydrofolate reductase, ubiquitin, β-lactamase, glycinamide ribonucleotide transformylase, hygromycin B, aminoglycoside kinase, aminoglycoside phosphotransferase, adenylate cyclase, CRE recombinase, GFP and related variants, and luciferase (reviewed in ref *43*). While disulfide cross-links are problematic for PCA, they may be advantageous in our design. If no disulfide bridge is present, then one can typically be introduced by rational placement of Cys residues.

ACKNOWLEDGMENT

We thank J.-H. Ha for discussions and the staff at the National Synchrotron Light Source (beamline X6A) and at the Cornell High Energy Synchrotron Source for beam time and assistance in data collection.

REFERENCES

1. Inobe, T., and Matouschek, A. (2008) Protein targeting to ATP-dependent proteases. *Curr. Opin. Struct. Biol. 18*, 43–51.
2. Sauer, R. T., Bolon, D. N., Burton, B. M., Burton, R. E., Flynn, J. M., Grant, R. A., Hersch, G. L., Joshi, S. A., Kenniston, J. A., Levchenko, I., Neher, S. B., Oakes, E. S. C., Siddiqui, S. M., Wah, D. A., and Baker, T. A. (2004) Sculpting the proteome with AAA+ proteases and disassembly machines. *Cell 119*, 9–18.
3. Ravid, T., and Hochstrasser, M. (2008) Diversity of degradation signals in the ubiquitin-proteasome system. *Nat. Rev. Mol. Cell Biol. 9*, 679–690.
4. Baird, G. S., Zacharias, D. A., and Tsien, R. Y. (1999) Circular permutation and receptor insertion within green fluorescent protein. *Proc. Natl. Acad. Sci. U.S.A. 96*, 11241–11246.
5. Perez-Jiminez, R., Garcia-Manyes, S., Ainavarapu, S. R. K., and Fernandez, J. M. (2006) Mechanical unfolding pathways of the enhanced yellow fluorescent protein revealed by single molecule force spectroscopy. *J. Biol. Chem. 281*, 40010–40014.
6. Viguera, A. R., Serrano, L., and Wilmanns, M. (1996) Different folding transition states may result in the same native structure. *Nat. Struct. Biol. 3*, 874–880.
7. Ivarsson, Y., Travaglini-Allocatelli, C., Brunori, M., and Gianni, S. (2008) Folding and misfolding in a naturally occurring circularly permuted PDZ domain. *J. Biol. Chem. 283*, 8954–8960.
8. Brinkmann, U., Di Carlo, A., Vasmatzis, G., Kurochkina, N., Beers, R., Lee, B., and Pastan, I. (1997) Stabilization of a recombinant F_v fragment by base-loop interconnection and V_H-V_L permutation. *J. Mol. Biol. 268*, 107–117.
9. Miller, E., Fischer, K. F., and Marqusee, S. (2002) Experimental evaluation of topological parameters determining protein-folding rates. *Proc. Natl. Acad. Sci. U.S.A. 99*, 10359–10363.
10. Kojima, M., and Ayabe, K. U. H. (2005) Importance of terminal residues on circularly permuted *Escherichia coli* alkaline phosphatase with high specific activity. *J. Biosci. Bioeng. 100*, 197–202.
11. Buchwalder, A., Szadkowski, H., and Kirschner, K. (1992) A fully active variant of dihydrofolate reductase with a circularly permuted sequence. *Biochemistry 31*, 1621–1630.
12. Goldenberg, D. P., and Creighton, T. E. (1983) Circular and circularly permuted forms of bovine pancreatic trypsin inhibitor. *J. Mol. Biol. 165*, 407–413.
13. Zhang, T., Bertelsen, E., Benvegnu, D., and Alber, T. (1993) Circular permutation of T4 lysozyme. *Biochemistry 32*, 12311–12318.
14. Luger, K., Hommel, U., Herold, M., Hofsteenge, J., and Kirschner, K. (1989) Correct folding of circularly permuted variants of a $\beta\alpha$ barrel enzyme *in vivo*. *Science 243*, 206–210.
15. Haglund, E., Lindberg, M. O., and Oliveberg, M. (2008) Changes of protein folding pathways by circular permutation: Overlapping nuclei promote global cooperativity. *J. Biol. Chem. 283*, 27904–27915.
16. Neira, J. L., Vázquez, E., and Fersht, A. R. (2000) Stability and folding of the protein complexes of barnase. *Eur. J. Biochem. 267*, 2859–2870.
17. Sancho, J., and Fersht, A. R. (1992) Dissection of an enzyme by protein engineering. The N and C-terminal fragments of barnase form a native-like complex with restored enzymatic activity. *J. Mol. Biol. 224*, 741–747.
18. Leuchtenberger, S., Perz, A., Gatz, C., and Bartsch, J. W. (2001) Conditional cell ablation by stringent tetracycline-dependent regulation of barnase in mammalian cells. *Nucleic Acids Res. 29*, e76.
19. Bi, Y.-M., Rothstein, S. J., and Wildeman, A. G. (2001) A novel strategy for regulated expression of a cytotoxic gene. *Gene 279*, 175–179.

20. Jacobson, G. R., Schaffer, M. H., Stark, G. R., and Vanaman, T. C. (1973) Specific chemical cleavage in high yield at the amino peptide bonds of cysteine and cystine residues. *J. Biol. Chem. 248*, 6583–6591.
21. Pace, C. N., and Scholtz, J. M., Eds. (1997) *Protein structure: A practical approach*, 2nd ed., Oxford University Press, New York.
22. Rushizky, G. W., Greco, A. E., Hartley, R. W., and Sober, H. A. (1963) Studies on *B. subtilis* ribonuclease. I. Characterization of enzymatic epecificity. *Biochemistry 2*, 787–793.
23. Otwinowski, Z., and Minor, W. (1997) Processing of X-ray Diffraction Data Collected in Oscillation Mode. *Methods Enzymol. 276*, 307–326.
24. McCoy, A. J. (2007) Solving structures of protein complexes by molecular replacement with Phaser. *Acta Crystallogr. D63*, 32–41.
25. Brunger, A. T., Adams, P. D., Clore, G. M., DeLano, W. L., Gros, P., Grosse-Kunstleve, R. W., Jiang, J. S., Kuszewski, J., Nilges, M., Pannu, N. S., Read, R. J., Rice, L. M., Simonson, T., and Warren, G. L. (1998) Crystallography & NMR system: A new software suite for macromolecular structure determination. *Acta Crystallogr. D54*, 905–921.
26. Emsley, P., and Cowtan, K. (2004) Coot: Model-building tools for molecular graphics. *Acta Crystallogr. D60*, 2126–2132.
27. Painter, J., and Merritt, E. A. (2006) Optimal description of a protein structure in terms of multiple groups undergoing TLS motion. *Acta Crystallogr. D62*, 439–450.
28. Painter, J., and Merritt, E. A. (2005) A molecular viewer for the analysis of TLS rigid-body motion in macromolecules. *Acta Crystallogr. D61*, 465–471.
29. Collaborative Computational Project Number 4 (1994) The CCP4 suite: Programs for protein crystallography. *Acta Crystallogr. D50*, 760–763.
30. DeLano, W. L. (2002) The PyMOL Molecular Graphics System, DeLano Scientific, San Carlos, CA.
31. Mauguen, Y., Hartley, R. W., Dodson, E. J., Dodson, G. G., Bricogne, G., Chothia, C., and Jack, A. (1982) Molecular structure of a new family of ribonucleases. *Nature 297*, 162–164.
32. Scalley-Kim, M., Minard, P., and Baker, D. (2003) Low free energy cost of very long loop insertions in proteins. *Protein Sci. 12*, 197–206.
33. Chan, H. S., and Dill, K. A. (1988) Intrachain loops in polymers. *J. Chem. Phys. 90*, 492–509.
34. Cutler, T., Mills, B. M., Lubin, D. J., Chong, L. T., and Loh, S. N. (2009) Effect of interdomain linker length on an antagonistic folding-unfolding equilibrium between two protein domains. *J. Mol. Biol. 386*, 854–868.
35. Kuhlman, B., O'Neill, J. W., Kim, D. E., Zhang, K. Y., and Baker, D. (2001) Conversion of monomeric protein L to an obligate dimer by computational protein design. *Proc. Natl. Acad. Sci. U.S.A. 98*, 10687–10691.
36. Patel, S. D., Chen, C. P., Bahna, F., Honig, B., and Shapiro, L. (2003) Cadherin-mediated cell-cell adhesion: Sticking together as a family. *Curr. Opin. Struct. Biol. 13*, 690–698.
37. Radley, T. L., Markowska, A. I., Bettinger, B. T., Ha, J.-H., and Loh, S. N. (2003) Allosteric switching by mutually exclusive folding of protein domains. *J. Mol. Biol. 332*, 529–536.
38. Santoro, M. M., and Bolen, D. W. (1988) Unfolding free energy changes determined by the linear extrapolation method. 1. Unfolding of phenylmethanesulfonyl α chymotrypsin using different denaturants. *Biochemistry 27*, 8063–8068.
39. Ha, J.-H., Butler, J. S., Mitrea, D. M., and Loh, S. N. (2006) Modular enzyme design: Regulation by mutually exclusive protein folding. *J. Mol. Biol. 357*, 1058–1062.
40. Johnson, R. J., Lin, S. R., and Raines, R. T. (2006) A ribonuclease zymogen activated by the NS3 protease of the hepatitis C virus. *FEBS J. 273*, 5457–5465.
41. Plainkum, P., Fuchs, S. M., Wiyakrutta, S., and Raines, R. T. (2003) Creation of a zymogen. *Nat. Struct. Biol. 10*, 115–119.
42. Turcotte, R. F., and Raines, R. T. (2008) Design and characterization of an HIV-specific ribonuclease zymogen. *AIDS Res. Hum. Retroviruses 24*, 1357–1363.
43. Michnick, S. W., Ear, P. H., Manderson, E. N., Remy, I., and Stefan, E. (2007) Universal strategies in research and drug discover based on protein-fragment complementation assays. *Nat. Rev. Drug Discovery 6*, 569–582.
44. Guillet, V., Lapthorn, A., Hartley, R. W., and Mauguen, Y. (1993) Recognition between a bacterial ribonuclease, barnase, and its natural inhibitor, barstar. *Structure 1*, 165–176.

BI900039E